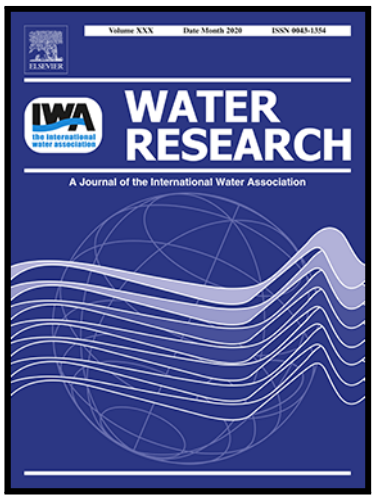

Exposure of Nanoplastics to Freeze-Thaw Leads to Aggregation and Reduced Transport in Model Groundwater Environments

OLUBUKOLA S. ALIMI , JEFFREY M. FARNER , NATHALIE TUFENKJI

PII: S0043-1354(20)31068-X
DOI: https://doi.org/10.1016/j.watres.2020.116533
Reference: WR 116533

To appear in: *Water Research*

Received date: 30 June 2020
Revised date: 12 October 2020
Accepted date: 16 October 2020

Please cite this article as: OLUBUKOLA S. ALIMI , JEFFREY M. FARNER , NATHALIE TUFENKJI , Exposure of Nanoplastics to Freeze-Thaw Leads to Aggregation and Reduced Transport in Model Groundwater Environments, *Water Research* (2020), doi: https://doi.org/10.1016/j.watres.2020.116533

Highlights

- First report on the effect of freeze-thaw on the fate of nanoplastics.
- Nanoplastics exposed to freeze-thaw formed aggregates and were less mobile.
- Natural organic matter increased particle mobility but did not prevent aggregation.
- The nanoplastic aggregates were not prone to disaggregation.
- Climate and temperature changes can impact plastic exposure risks.

Exposure of Nanoplastics to Freeze-Thaw Leads to Aggregation and Reduced Transport in Model Groundwater Environments

OLUBUKOLA S. ALIMI, JEFFREY M. FARNER and NATHALIE TUFENKJI*

Department of Chemical Engineering, McGill University,

Montreal, Quebec H3A 0C5, Canada

* Corresponding Author. Phone: (514) 398-2999; Fax: (514) 398-6678; E-mail: nathalie.tufenkji@mcgill.ca

Abstract

Despite plastic pollution being a significant environmental concern, the impact of environmental conditions such as temperature cycling on the fate of nanoplastics in cold climates remains unknown. To better understand nanoplastic mobility in subsurface environments following freezing and thawing cycles, the transport of 28 nm polystyrene nanoplastics exposed to either constant (10 °C) temperature or freeze-thaw (FT) cycles (-10 °C to 10 °C) was investigated in saturated quartz sand. The stability and transport of nanoplastic suspensions were examined both in the presence and absence of natural organic matter (NOM) over a range of ionic strengths (3-100 mM NaCl). Exposure to 10 FT cycles consistently led to significant aggregation and reduced mobility compared to nanoplastics held at 10 °C, especially at low ionic strengths in the absence of NOM. While NOM increased nanoplastic mobility, it did not prevent the aggregation of nanoplastics exposed to FT. We compare our findings with existing literature and show that nanoplastics will largely aggregate and associate with soils rather than undergo long range transport in groundwater in colder climates following freezing temperatures. In fact, FT exposure leads to the formation of stable aggregates that are not prone to disaggregation. As one of the first studies to examine the coupled effect of cold temperature and NOM, this work highlights the need to account for climate and temperature changes when assessing the risks associated with nanoplastic release in aquatic systems.

Keywords

microplastics; natural organic matter; colloid transport; porous media; plastic pollution; climate change

1. Introduction

Plastic pollution is one of the major environmental challenges of the 21st century with recent evidence highlighting the potential risk in terrestrial and freshwater ecosystems (Koelmans et al., 2019; Pivokonsky et al., 2018). Plastics have been detected in almost every environmental compartment (Law et al., 2010; Nizzetto et al., 2016; Panko et al., 2013; Zubris and Richards, 2005) and will degrade over time due to various environmental stresses to produce smaller, secondary, plastic particles such as microplastics (100 nm–5 mm in size) and nanoplastics (<100 nm) (Alimi et al., 2018; Andrady, 2011; Mattsson et al., 2015). Additionally, some products containing intentionally produced (primary) microplastics have been shown to also include nanoplastics (Hernandez et al., 2017). Although the fate of plastics in soils has received less attention, recent studies suggest that soils may be a larger reservoir for and source of plastics than other environmental compartments (Duis and Coors, 2016; Hurley and Nizzetto, 2018). Nanoplastics released from surface water run-off, landfill storage and agricultural activities such as biosolids application and plastic mulch may end up in soils which could contaminate drinking water supplies via infiltration into groundwater. Thus, understanding the transport potential of nanoplastics in soils and aquifers is crucial to protecting human and environmental health.

The transport potential of nanoplastics and other nanoparticles in groundwater is typically assessed by measuring the amount of particles retained in laboratory based saturated porous media that mimic groundwater environments (Petosa et al., 2010; Quevedo and Tufenkji, 2012; Tufenkji and Elimelech, 2004). Several physicochemical factors that are associated with properties of the nanoplastic (e.g., size, surface functionalization), porous medium (grain size, geochemistry), pore water chemistry (pH, presence of organic matter, ionic strength), and hydrological conditions (flow velocity) have been shown to affect the transport of nanoplastics in

saturated porous media (Alimi et al., 2018; Bradford and Bettahar, 2006; Bradford et al., 2002; Pelley and Tufenkji, 2008; Petosa et al., 2010). The effect of temperature or freezing which could age or transform nanoplastic suspensions, however, has largely been overlooked. Most nanoplastic transport experiments have been conducted under ambient temperature conditions (20–25 °C) (Alimi et al., 2018). Some studies have employed the typical range of groundwater temperatures (4–20 °C), however they do not cover cycles of freezing and thawing temperatures experienced in colder climates (Bense and Kooi, 2004; Kim and Walker, 2009; Quevedo and Tufenkji, 2012; Sasidharan et al., 2017). From theory, the mass transfer rate of particles from bulk solution to the grain surface (described by the single-collector contact efficiency, η_0) should decrease at lower temperatures due to a decrease in the diffusion coefficient, and thus cold climate regions might face higher risks of nanoplastic exposure to drinking water wells due to the higher particle mobility observed at lower temperatures (Kim and Walker, 2009; Sasidharan et al., 2017; Yan et al., 2014). This temperature-dependent behavior has also been observed with other colloids, such as graphene oxide (Wang et al., 2018), bacteriophage (Bales et al., 1997) and *E. coli* (Castro and Tufenkji, 2007).

Beyond simple cold temperatures, many parts of the world experience cycles of freezing and thawing in early and late winter. Exposure to freeze-thaw (FT) cycling has been associated with changes in bacterial virulence and transport in porous media (Asadishad et al., 2013; Asadishad et al., 2014; Hakimzadeh et al., 2018; Rocard et al., 2018), whereby contradictory results regarding enhanced or reduced mobility have been reported, depending on the bacterial species studied. In addition to the lack of clear trend, the transport behavior of biocolloids may be of limited use in predicting the mobility of non-biological colloids in saturated porous media, due to their unique features (e.g., cell hydrophobicity, motility, cell surface appendages)

(Asadishad et al., 2013; Rocard et al., 2018) which may introduce additional transport and attachment mechanisms not considered in traditional filtration theory. A recent study investigating titanium dioxide (TiO_2) nanoparticles demonstrated that FT induced aggregation, increased deposition, and limited particle transport (Farner et al., 2020). While the presence of NOM has generally been reported to stabilize particle suspensions at room temperature, thereby increasing particle mobility in porous media, TiO_2 subjected to FT in the presence of NOM was associated with larger, more irreversibly agglomerated particles (Farner et al., 2020). Currently, there is no information on the impact of FT on nanoplastic transport in the environment or on the interaction between NOM and nanoplastic during and after FT. Within other contexts such as quality control, biological applications, etc., freeze-thaw has been employed to test suspension stability of colloids (Barb and Mikucki, 1959; Chou et al., 2014). For example, Barb and Mikucki reported that frozen suspensions of 50–100 nm polystyrene latex particles remained agglomerated even after thawing at room temperature (Barb and Mikucki, 1959). Understanding the effect of FT on nanoplastic transport in model groundwater environments will be beneficial in risk assessments, especially for climates that experience repeated FT cycling (Law et al., 2010).

In this study, we systematically examined the influence of FT cycles on the transformations and transport of model primary nanoplastics in saturated porous media at a groundwater temperature relevant to southern Canada. Nanoplastic stability and transport were investigated over a range of ionic strengths (IS) in monovalent salt, in both the presence and absence of NOM, at 10 °C and after exposure to 10 FT cycles. Under all conditions, 10 FT cycles led to significant aggregation and reduced mobility compared to nanoplastics held at 10

°C. Although the presence of NOM increased nanoplastic mobility in column tests, it did not prevent the aggregation of nanoplastics exposed to FT.

2. Materials and Methods

2.1. Nanoplastic and natural organic matter suspension preparation

Carboxylate-modified polystyrene latex Fluospheres® of 28 nm nominal diameter (Molecular Probes, Invitrogen) were used to represent model primary nanoplastics. The stock suspension (approximate number concentration of 4.5×10^{15} particles/mL) was bath sonicated for 3 min before the preparation of each working suspension. For transport and characterisation experiments, the stock suspension was diluted to an initial working concentration of 2 mg nanoplastics/L (~2.3×10^{11} particles/mL) at pH 6.0 ± 0.2 in various electrolyte solutions ranging from 3-100 mM IS in either the presence or absence of NOM. All electrolyte solutions were prepared using analytical grade NaCl (Fisher Scientific) in filtered reverse osmosis water (Biolab Scientific), and the pH was adjusted with 0.01M NaOH and HCl. Suwannee river NOM (International Humic Substances Society, RO Isolate, 2R101N) was used as a representative NOM. A stock solution of 100 mg/L NOM was prepared in reverse osmosis water, adjusted to pH 8, stirred overnight, and stored in the dark at 4 °C. This stock was spiked into suspensions at 5 mg/L for experiments conducted in the presence of NOM. Each working suspension was then vortexed for approximately 20 s to obtain a well-dispersed suspension and subjected to one of two temperature pre-treatments: either kept at 10 °C (control) for 10 days or exposed to 10 FT cycles. Prior to each experiment, the suspension was gently inverted to resuspend any settled nanoplastics.

2.2. Temperature Pre-treatments

Natural FT cycles were simulated in a recirculating chiller (Julabo CORIO CD-200F) filled with a 70/30 ratio of water/propylene glycol. The temperature profile (Fig. S1) was selected to represent southern Quebec, Canada during the winter shoulder periods (Asadishad et al., 2013; Hakimzadeh et al., 2018). Nanoplastic working suspensions were exposed to 10 FT cycles of 24 h each. During each FT cycle, the temperature was brought from +10 to -10 °C over 8 h, held at -10 °C for 4 h, brought back to +10 °C over 8 h, and then held at 10 °C for 4 h. In the second pre-treatment, samples were kept at a constant temperature of 10 °C for the same duration (240 h).

In separate experiments, nanoplastic suspensions in 10 mM NaCl were exposed to 1, 5, and 10 FT cycles to examine the effect of the number of FT cycles. The stability of the suspension after each treatment was then monitored over 5 days. For each stability test, the nanoplastic suspension was gently shaken (moderate shearing force applied to not exceed the low flowrate expected in groundwater) before each measurement. A separate stability test where the suspension was vigorously mixed for 30 s using a vortexer at 100 rpm each day post FT was also performed.

2.3. Nanoplastic Characterization

Nanoplastic suspensions were characterized following temperature pre-treatments. Nanoplastics and aggregate sizes were determined using dynamic light scattering (DLS) and transmission electron microscopy (TEM), while the zeta potential (ZP), which is an estimation of surface

charge, was determined from the electrophoretic mobility measured by laser Doppler velocimetry. The electrophoretic mobility measurements were converted to ZP using the Smoluchowski approximation with the Henry equation (Lowry et al., 2016). Both DLS and laser Doppler velocimetry measurements were conducted using a Malvern Zetasizer Nano (Malvern Panalytical). For DLS measurements, the Z-average diameter ($d_{h,\ Z\text{-}avg}$) (cumulants mean diameter), intensity mean diameter ($d_{h,\ intensity}$) and volume mean diameter ($d_{h,\ volume}$) are reported. The polydispersity index (PDI) provides an indication of the heterogeneity of aggregate sizes within a suspension and ranges from 0 (monodisperse) to 1 (highly polydisperse). Aggregate morphology and primary particles were visualized using TEM (FEI Technai 120 kV TEM coupled with a Gatan Ultrascan 4000 4k×4k CCD camera. TEM was performed on suspensions deposited onto thin carbon film grids (Pacific Grid-Tech, 300 mesh, 3.05 mm O.D., hole size) and allowed to dry at room temperature after wicking away the excess liquid with a Whatman filter paper.

2.4. Nanoplastic Transport Studies

Column experiments were performed at 10 °C inside a cold chamber (Danby, DWC032A2BDB), analogous to previous studies (Farner et al., 2020; Mitzel et al., 2016; Pelley and Tufenkji, 2008; Quevedo and Tufenkji, 2012; Rocard et al., 2018). Glass chromatography columns (16 mm inner diameter, GE Life Sciences) were packed with high purity fine quartz sand (-50 +70 mesh size, d_{50} = 256 μm, Sigma-Aldrich). The sand was acid-washed before use following the protocol of Pelley and Tufenkji (Pelley and Tufenkji, 2008). Prior to each column experiment, 26 g of sand was soaked in the desired electrolyte for a minimum of 10 days at 10 °C and then wet packed into the glass columns. Uniform packing of the sand bed was ensured by gentle vibration which resulted in a final packed bed length of 85 mm. The porous media was supported by a Nylon

Spectra mesh filter (pore size: 70 µm, thickness 70 µm). One pore volume (PV) was calculated by subtracting the volume of the sand used (density = 2.6 g/cm^3) from the total volume of the packed column and confirmed using 0.01 M KNO_3 as a tracer. The column porosity, calculated as one PV divided by the total volume of the packed column, was 0.43. After packing, a minimum of 10 PVs of electrolyte solution were pumped through the porous medium to equilibrate the column. For experiments including NOM, the column was equilibrated with electrolyte containing 5 ppm NOM. Electrolyte and nanoplastic suspensions were introduced at a constant approach velocity of 7.5×10^{-5} m/s using syringe pumps (Kd Scientific). For deposition experiments, 5 PVs of nanoplastics suspension were injected into the column followed by the particle-free electrolyte until almost no nanoplastics were detected in the effluent. Influent (C_0) and effluent (C) nanoplastic concentrations were collected in real-time by spectrofluorometry (FluoroMax-4 Jobin Yvon Horiba, Edison, NY), where C_0 was measured before each column experiment and by bypassing the sand column. The nanoplastic excitation (505 nm) and emission (515 nm) wavelengths were provided by the nanoplastic manufacturer and verified in the laboratory.

2.5. Interpreting Transport Experiments

To compare nanoplastic transport across treatments, the particle attachment efficiency, α, was calculated using the influent sizes measured by DLS and the average C/C_0 determined from the numerical integration of the area under the breakthrough curve (BTC, plotted as C/C_0 versus PV) using Equation 1 (Tufenkji and Elimelech, 2004; Yao et al., 1971):

$$\alpha = -\frac{2}{3}\frac{d_c}{(1-\theta)L\eta_0} ln\left[\frac{C}{C_0}\right] \quad (1)$$

where L is the length of the packed filter medium, θ is the porosity of the sand bed, d_c is the average diameter of the sand grains, and C/C_0 is calculated by integrating the experimental particle BTCs. A detailed explanation can be found in Tufenkji and Elimelech, 2004.

3. Results and discussion

3.1. Physicochemical Properties of Nanoplastics Exposed to Freeze-Thaw

One of the key factors determining the fate of nanoplastics in porous media is the particle size (Alimi et al., 2018). The hydrodynamic diameters (d_h) of nanoplastics at 10 °C and after exposure to FT are reported as the Z-average ($d_{h,\ z\text{-}avg}$), intensity mean ($d_{h,\ intensity}$), and volume mean ($d_{h,\ volume}$) diameters in Table 1.

<Insert Table 1 here>

For monodisperse particle suspensions, $d_{h,z\text{-}avg}$ and $d_{h,intensity}$ will be the same, and either measurement would accurately describe the particle size in suspension. However, DLS becomes less accurate when the polydispersity index (PDI) is high (> 0.5). Under these conditions, the Z-average diameter, calculated from the method of cumulants, may overestimate d_h since the scattering intensity is proportional to the sixth power of the particle diameter (Domingos et al., 2009). In such cases, the intensity peak may be more accurate in describing the system as it is the closest distribution to what is measured (Bhattacharjee, 2016; Farner et al., 2019).

From Table 1, measured values of the influent $d_{h,\ intensity}$ at 10 °C ranged from 55±4 – 80±3 nm in 3–100 mM IS. These values, together with the PDI (≤ 0.36), suggest that the particles are generally stable under all conditions (at 10 °C) examined, even at high IS (100 mM NaCl). It is worth noting that the nanoplastic manufacturer suggests that the carboxylate-modified nanoplastics are stable in up to 1 M monovalent salt (Probes, 2004). Inspection of the intensity-based particle size distribution (PSD) of the nanoplastics at 10 °C, (Fig. 1a and b, Fig. S2 open red squares) reveals that the PSD is reproducible across triplicate runs. In the presence of NOM (solid symbols), the nanoplastics are also stable at 10 °C. The PSD of the pristine nanoplastics at 10 °C occasionally indicated the presence of some aggregates greater than 2000 nm comprising ~1–10 % of the total particle population. Because even a small trace of large aggregates or artifacts will skew the intensity mean, the intensity weighted diameter peak with at least 90% of the particle population was reported as the $d_{h,intensity}$ (Table 1) in such cases (refer to section S2 for further discussion) (Malvern, 2011). The calculated volume mean diameter is in good agreement with this 90% intensity peak (see Fig. S3 for comparison). The $d_{h,intensity}$ and $d_{h,z\text{-}}$

$_{avg}$ values observed in this study were ~2 times larger than the nominal size (~28 nm) reported by the manufacturer and obtained via TEM. This is not surprising, as DLS hydrodynamic sizes are usually greater than those observed with TEM (Bhattacharjee, 2016; Domingos et al., 2009). Indeed, size analysis of TEM images for the stable nanoplastics at 10 °C (Fig. 1 c and d) reveal sizes similar to the manufacturer's report (25 ± 4 nm, n = 48 as determined via Image J analysis).

<Insert Fig. 1 here>

Suspensions exposed to 10 FT cycles underwent aggregation that caused significant shifts in the PSD from 10–100 nm towards larger sizes of 100–1000 nm or greater (Fig. 1a and b, blue circles). The presence of NOM did not prevent the aggregation of nanoplastics following FT, and size ranges are on same order of magnitude for nanoplastics in the absence of NOM. For example, in 30 mM, the bare nanoplastics have $d_{h,intensity}$ = 687 ± 124 while in the presence of NOM, $d_{h,intensity}$ = 483 ± 121 (Table 1). TEM images confirm the formation of large aggregates upon exposure to repeated FT cycles (Fig. 1c-f).

The effects of 3 different pre-treatment durations (1, 5, or 10 FT cycles) on the $d_{h,\,z\text{-}avg}$ of the aggregates as well as on the disaggregation behavior of the aggregates were investigated. Fig. 2 shows the $d_{h,\,z\text{-}avg}$ of the aggregates before and after the 3 pre-treatments. After exposure to all 3 pre-treatments, the hydrodynamic size increased to ~2000 nm and remain aggregated after 5 days. The aggregate size for the 1 FT cycle suspension post FT slightly decreased over the 5 days but did not fall below ~1000 nm (Fig. 2a). For all cycles, vigorously mixing the suspension did not result in an appreciable decrease in $d_{h,\,z\text{-}avg}$ compared to day 5 post FT. This suggests that

the aggregates formed after exposure to FT may be stable over longer time periods. Overall, the DLS measurements indicate that exposure to FT leads to formation of aggregates that can be stable but highly polydisperse.

<Insert Fig. 2 here>

Table 1 lists the ZP of nanoplastics in NaCl before and after FT treatment as well as in the presence and absence of NOM. All particles were negatively charged at pH 6 as anticipated given the carboxylic functional groups. The ZP was generally unchanged by increasing IS at 10 °C, except for nanoplastic suspensions in 100 mM IS (-15.2 ±1.1 mV). This is seen both in the presence and absence of NOM which can be attributed to the screening of the electrical double layer as salt concentration increases. For bare nanoplastics, exposure to 10 FT cycles moderately impacted the ZP when compared with those kept at 10 °C.

The ZP of nanoplastics in 30 mM NaCl and the presence of NOM (-55.5 ± 7.2 mV) was more negative compared to nanoplastics in the absence of NOM (-22.5 ± 5.9 mV). This was also generally observed for nanoplastics subjected to FT in the presence of NOM, although no differences in ZP are observed in 100 mM NaCl. The carboxyl and hydroxyl functional groups present in NOM will impart negative charges on microplastics and nanoplastics, leading to more negative ZPs (Franchi and O'Melia, 2003; Pelley and Tufenkji, 2008; Song et al., 2019). We also observed some differences in ZP for the NOM coated nanoplastics when exposed to FT versus 10 °C. For example, after 10 FT cycles, nanoplastics in 30 mM IS + NOM, had a less negative ZP (-34.9±9.3 mV) compared to those not exposed to FT (-55.5±7.2 mV). It is important to note

that the ZP values for the NP aggregates should be considered with caution as the aggregates are not solid spheres (see Figure 1).

3.2. Proposed mechanism of aggregation upon exposure to freeze-thaw

The formation of large aggregates after exposure to 10 FT cycles occurred irrespective of IS. This is also observed in the presence of NOM, which has been shown to stabilize nanoplastics and other colloids even at high monovalent IS (Pelley and Tufenkji, 2008; Saleh et al., 2010). Previously, FT has been used to intentionally induce the aggregation of nanoparticles (Chou et al., 2014). Similarly, Xiang *et al.* found only cryoprotectants (e.g. polyethylene glycols, Tween 20) to be effective in preventing FT induced aggregation of proteins (Xiang et al., 2015). We therefore hypothesize that aggregation is due to the solute rejection phenomenon in which the ordered crystalline structure of ice rejects impurities (e.g., insoluble particles) during freezing (Halde, 1980). This increases the local concentration of nanoplastics in the still-unfrozen water (Barb and Mikucki, 1959; Halde, 1980), inducing aggregation. When the ice thaws, particles remain aggregated.

3.3. Nanoplastic Transport in the Absence of Freeze-Thaw

Fig. 3 shows the BTCs for transport experiments conducted in the presence and absence of NOM. In agreement with DLVO theory (Derjaguin and Landau, 1993; Verwey et al., 1948), nanoplastic deposition increased with IS. Considerable transport (C/C_0 = 0.95 and 0.72) is

observed at low IS (3 and 10 mM NaCl, respectively) (Fig. 3a). However, as IS increases to 30 and 100 mM, nearly all particles are retained in the column (C/C_0 = 0.024 and 0.026, respectively). Although the size and ZP of the bare nanoplastics in this study are not greatly impacted by increasing IS up to 30 mM (Table 1), the ZP of the quartz sand collector in the column has been shown to vary with IS: -18.9±0.3 mV in 1 mM NaCl vs -12.7±0.5 mV in 10 mM NaCl (Mitzel et al., 2016). The ZP of the sand grain continuing to approach zero with increasing IS would explain the favorable deposition despite the similar ZP values of the nanoplastics themselves.

<Insert Fig. 3 here>

It is worth noting the different shapes of the BTCs (Fig. 3a and b) – which can give insight into the governing type of deposition mechanism in the porous medium. Typical BTCs observed in colloid transport studies are either constant, increasing (due to blocking) or decreasing (indicative of straining and/or ripening) with time (Liu et al., 1995). Blocking occurs when deposited particles prevent subsequent deposition of incoming particles. Colloids may become physically strained when entrapped in smaller pores between grains, thereby clogging the pores and reducing elution over time. Ripening is a result of multi-layer deposition in which incoming particles are retained on already deposited particles (Liu et al., 1995). In some cases, (e.g., 100 mM NaCl + NOM, Fig. 3b), the BTCs exhibit a pronounced shape that is characteristic of blocking. Similarly, Quevedo and Tufenkji observed increasing BTCs indicative of blocking with 24 nm nanoplastics in 10 mM KCl using the same sand grains (Quevedo and Tufenkji,

2012). Similar behavior was observed by researchers working with cerium dioxide nanoparticles (Petosa et al., 2013).

To investigate how the presence of NOM, which is ubiquitous in the environment, would influence transport, 5 mg/L of NOM was added to nanoplastics suspensions of 30 and 100 mM IS. Fig. 3b compares the BTCs in the presence (closed symbols) versus absence (open symbols) of NOM at 10 °C. As previously discussed, bare nanoplastics show almost no elution through the column at 30 mM and 100 mM IS; however, nanoplastic mobility increased significantly in the presence of NOM. Increased retention is observed at 100 mM (C/C_0=0.54) compared to 30 mM (C/C_0=0.92) which is in agreement with the DLVO theory and consistent with the ZP measured (-55.5±7.2 mV at 30 mM compared to -15.0±4.1 mV at 100 mM). At 100 mM, BTCs characteristic of blocking are observed, though not at 30 mM IS. Interestingly, values of C/C_0 in 30 mM IS + NOM are similar to bare nanoplastics in 3 mM IS (0.95 and 0.92, respectively). This highlights the ability of NOM to increase nanoplastic mobility, even at high IS (typical groundwater IS may reach up to 10 mM monovalent ions and 2 mM divalent ions (Busenberg et al., 2000), and agrees with previous studies (Deshiikan et al., 1998; Petosa et al., 2010; Song et al., 2019). This has been observed in a natural groundwater where suspended organic matter increased the mobility of 50 nm carboxylated nanoplastics compared to the same groundwater where the organic matter had been previously removed (Song et al., 2019). The interaction between NOM and carboxylated PS has been well studied in the literature (Wu et al., 2019; Yu et al., 2019). NOM interacts with surfaces via electrostatic interaction, hydrophobic interaction or ligand exchange which imparts electrosteric, electrostatic or steric stability on negatively charged nanoparticles (Aiken et al., 2011; Franchi and O'Melia, 2003; Philippe and Schaumann, 2014). In one particularly relevant recent work, the authors demonstrated significant adsorption

of Suwannee River NOM onto PS-COOH using initial NOM concentrations between 1 – 10 mg C/L (Yu et al., 2019). This range covers the concentration used in this study (2.6 mg C/L). Additionally, the presence of NOM on sand surfaces has been reported to impart steric stabilization, significantly reducing particle retention (Johnson and Logan, 1996). Thus, the stabilizing effect observed at 30 and 100 mM (Fig. 3b) is not surprising.

3.4. Nanoplastic transport after exposure to 10 FT cycles

Exposure to FT (Fig. 3c) greatly decreases the transport of bare nanoplastics compared to controls held at 10 °C in 3 and 10 mM IS (Fig. 3a). This is likely due to the FT-induced aggregation of nanoplastics, resulting in greater deposition. At low IS of 3 and 10 mM, differences in nanoplastic transport can be linked to aggregate size. Nanoplastic aggregates in suspensions held at 10 °C are smaller ($d_{h,z\text{-}avg}$ of 55±2 nm and 46±4 nm, respectively) and more monodisperse than the suspensions exposed to FT (1044±156 nm and 582±331 nm, respectively). At 3 mM, C/C_0 reduces from 0.95 to 0.49 after FT exposure while at 10 mM, C/C_0 reduces from 0.72 to 0.47. At 30 and 100 mM IS, FT does not significantly impact nanoplastic transport as almost complete retention of nanoplastics is observed in the sand column for particles exposed to both temperature pretreatments, even though the particles exposed to FT treatment form much larger aggregates (668±85 and 612±353 nm, respectively) than those at 10 °C (46±10 and 58±4 nm, respectively) (Table 1). Physical straining is thought to become important when aggregate diameter (d_a) to collector diameter (d_c) ratios (d_a/d_c) are in the range of 0.002 to 0.008 or greater (Bradford et al., 2002; Xu et al., 2006), or when the collector shape is irregular and angular (Tufenkji et al., 2004), likely leading to an increase in particle retention.

For the 256 µm collector (grain size) used here, these ratios translate to an aggregate diameter range of 512-2048 nm or greater. Since all d_a in this work range from 384±32 – 2834±1585 nm (for FT exposed particles), straining is likely in some cases. However, a decrease in C/C_0 over time is not observed in all cases as would have been expected if physical straining was the dominant mechanism. Perhaps, some of the larger aggregates were entrapped in the pore spaces due to straining, but this does not appear to be the only reason for the difference between 10 °C and FT BTCs.

As was observed at 10 °C, nanoplastic mobility in 30 and 100 mM after FT was greater in the presence of NOM (Fig. 3d, solid symbols) compared to the absence (Fig. 3d, open symbols). This can be due to steric stabilization by the NOM as the nanoplastic aggregates form. However, even in the presence of NOM, FT reduces transport which is readily observed when each IS is compared with the equivalent 10 °C control (Fig. S4). Therefore, the increase in gravitational sedimentation, interception, and physical straining associated with larger aggregate size following FT outweighs the influence of steric stabilization.

3.5. Interpreting Transport Experiments

Attachment efficiencies, α, calculated from Equation 1, are reported in blue and red symbols using both $d_{h,z\text{-}avg}$ (Fig. 4a) and $d_{h,intensity}$ (Fig. S5b) (Table 1). The influence of aggregate size is observed in the slight differences in reported α values; however, both calculated $\alpha_{z\text{-}avg}$ and $\alpha_{int\text{-}mean}$ exhibit the same trend (See Fig. S5). Thus, we focus on $\alpha_{z\text{-}avg}$ in this discussion. The stability curves show qualitative agreement with the DLVO theory whereby α generally increases with IS. For bare nanoplastics at 10 °C, $\alpha_{z\text{-}avg}$ varied over two orders of magnitude (~$0.004 < \alpha < 0.25$) in

the range of 3–100 mM NaCl IS. Even at 100 mM IS, $\alpha_{z\text{-}avg}$ does not approach unity, the point at which particles would be completely destabilized.

<Insert Fig. 4 here>

For nanoplastics exposed to FT (blue symbols), $\alpha_{z\text{-}avg}$ is significantly higher with more remarkable differences at low IS of 3 and 10 mM when compared to the 10 °C controls. The difference in $\alpha_{z\text{-}avg}$ for nanoplastics exposed to FT versus 10 °C in 30 and 100 mM is nearly an order of magnitude (Fig. 4a).. Overall, the differences in $\alpha_{z\text{-}avg}$ highlight the importance of considering FT-induced nanoplastic aggregation when making predictions of nanoplastic transport in cold climates. Under all conditions examined, the presence of NOM significantly reduced the $\alpha_{z\text{-}avg}$ of the nanoplastics. This is consistent with previous studies that have examined the effect of NOM on α (Deshiikan et al., 1998; Franchi and O'Melia, 2003; Pelley and Tufenkji, 2008).

The current results are compared with previous studies using quartz sand grains with similar sizes and conducted with negatively charged nanoplastics and microplastics (Fig. 4a). The α values reported by Quevedo and Tufenkji are generally lower than this study even though the nanoplastics are relatively the same size and functionalization from the same manufacturer (Quevedo and Tufenkji, 2012). This can be attributed to the higher pH (pH 7 in their study compared to pH 6 in this study) resulting in significantly larger particle ZPs (-64 mV to -34 mV for 0.1 to 100 mM KCl IS). At 30 and 100 mM IS, the stability curve for 50 nm sulfonated nanoplastics reported by Pelley and Tufenkji at 20 °C is comparable with that at 10 °C in this study (Pelley and Tufenkji, 2008; Quevedo and Tufenkji, 2012). Both studies were carried out at comparable pH but with different particle surface functionalization and size. This explains

differences in the ZP (approximately -50 mV to -30 mV for 1-100 mM KCl IS) which is greater than the ZP measured in this work (-25.5±5.4 mV to -15±2 mV for 1-100 mM NaCl IS). The work of Mitzel *et al.* shows lower α values compared to this study especially at 10 mM and for the carboxyl functionalized nanoplastics. Although Mitzel *et al.* used similarly sized nanoplastics, they worked at pH 7 with larger quartz sand grains. In their work, the ZP of the nanoplastics ranged between -57 mV to -43 mV. Kim and Walker investigated the effect of changing temperatures on the transport of 1000 nm carboxylate PS microplastics in 10 mM KCl and found that α decreased in the order 25 °C > 10 °C ≈ 4 °C (Kim and Walker, 2009). These α values especially at 25 °C are all higher than this work at 10 °C, however the α of nanoplastics exposed to FT are higher than those reported by Kim and Walker. Indeed, when comparing apparent α values at 10 mM, nanoplastics exposed to FT in this work are higher than other reports, which span 3 orders of magnitude. When considering factors that affect α, we show here that FT has an equal or greater influence on the apparent α. While these studies (Fig. 4a) have been conducted under several different conditions that make direct comparison difficult, they highlight the significant effect of FT on nanoplastic mobility in model groundwaters.

The predicted particle travel distance can be defined as the depth of packed sand that is required to remove 99.9% of the nanoplastics from the fluid phase and can be used to estimate potential nanoplastic exposures in subsurface environments (Fig. 4b). Travel distances were calculated using the experimentally determined $\alpha_{z\text{-}avg}$ in Table 1 (see Section S6 for equation). For the conditions studied, the greatest travel distance was 10 m for bare nanoplastics at 3 mM IS. We observe a decrease in the travel distance of nanoplastics after exposure to 10 FT cycles at low IS. Following FT, calculated travel distances did not exceed 1 m for any condition. As IS increases, the travel distance for bare nanoplastics exposed to FT and 10 °C converge as the

nanoplastics are already destabilized from the high electrolyte concentration. The IS at which this occurs is shifted to higher concentrations in the presence of NOM.

4. Conclusions

Recent evidence has confirmed the presence of microplastics in groundwater and drinking water from groundwater sources (Mintenig et al., 2019; Panno et al., 2019), and the prevalence of nanoplastics, though still unknown, is likely. Meanwhile, the effect of freeze-thaw on the mobility of nanoplastics in the subsurface environment has been largely overlooked. Previous literature looking at warm and cold – though not freezing – temperatures has suggested that drinking water wells in colder climates are at higher risk of nanoplastic and other nanomaterial contamination due to the higher particle mobility observed at lower temperatures (Elimelech et al., 1995; Kim and Walker, 2009; Sasidharan et al., 2017; Wang et al., 2018). Repeated freeze-thaw cycles are an important weather feature experienced in cold climates with some parts of the world having up to 105 FT cycles annually (NOAA/NCDC, 2000). Our results, in which exposure of nanoplastics to 10 FT cycles was shown to reduce transport under all conditions, suggest that nanoplastics are more likely to be associated with soils and less likely to undergo long range transport in groundwater in colder climates following freezing temperatures. This has implications in a broader context as emerging research shows that nanoplastics can act as transport vehicles for persistent organic pollutants in saturated porous media (Panno et al., 2019). Consequently, this FT-induced change in nanoplastic transport might mitigate the mobility of these organic pollutants. We propose that the increase in retention following FT observed in this work was driven by the freezing-induced aggregation of nanoplastics in suspension. This was recently observed for TiO_2 nanoparticles where a single FT cycle induced

aggregation and reduced transport in otherwise stable suspensions (Farner et al., 2020). While the presence of NOM significantly increases nanoplastic mobility, it was not sufficient to counter the impact of FT. Stability tests show that the aggregates formed after FT exposure are not prone to disaggregate even after applying high shear stress, suggesting that they will be stable over longer time scales in the environment. By ignoring the impact of freezing temperatures, transport predictions may overestimate the travel distances of nanoplastics in cold climates. This highlights the need to account for weather patterns when assessing the risks associated with nanoplastic release in aquatic systems.

Conflicts of interest

There is no conflict of interest.

Acknowledgements

The authors acknowledge the financial support of the Canada Research Chairs program, the Natural Sciences and Engineering Research Council of Canada (NSERC), the Canada Foundation for Innovation, the Petroleum Technology Development Fund (PTDF) of Nigeria for an award to OSA, McGill University for a MEDA and Eugenie Ulmer-Lamothe award to OSA, and NSERC PURE CREATE for a scholarship to OSA.

Supporting Material Available:

Temperature profile (Fig. S1); Representative intensity based particle size distribution (Fig. S2); Comparison of intensity versus volume particle size distributions (Fig. S3).. Breakthrough curves

of nanoplastic at 30 and 100 mM highlighting the effect of freeze-thaw in the presence of NOM (Fig. S4). Z-average versus intensity size-based attachment efficiency comparison (Fig. S5). Predicted travel distance equation (Section S6). Parameters used in calculating attachment efficiency (Section S7).

Declaration of interests

☒ The authors declare that they have no known competing financial interests or personal relationships that could have appeared to influence the work reported in this paper.

☐The authors declare the following financial interests/personal relationships which may be considered as potential competing interests:

References

Aiken, G.R., Hsu-Kim, H. and Ryan, J.N. 2011. Influence of Dissolved Organic Matter on the Environmental Fate of Metals, Nanoparticles, and Colloids. Environ. Sci. Technol. 45(8), 3196-3201.

Alimi, O.S., Farner Budarz, J., Hernandez, L.M. and Tufenkji, N. 2018. Microplastics and nanoplastics in aquatic environments: Aggregation, deposition, and enhanced contaminant transport. Environ. Sci. Technol. 52(4), 1704-1724.

Andrady, A.L. 2011. Microplastics in the marine environment. Mar. Pollut. Bull. 62(8), 1596-1605.

Asadishad, B., Ghoshal, S. and Tufenkji, N. 2013. Role of cold climate and freeze-thaw on the survival, transport, and virulence of *Yersinia enterocolitica*. Environ. Sci. Technol. 47(24), 14169-14177.

Asadishad, B., Olsson, A.L., Dusane, D.H., Ghoshal, S. and Tufenkji, N. 2014. Transport, motility, biofilm forming potential and survival of *Bacillus subtilis* exposed to cold temperature and freeze-thaw. Water Res. 58, 239-247.

Bales, R.C., Li, S., Yeh, T.C.J., Lenczewski, M.E. and Gerba, C.P. 1997. Bacteriophage and microsphere transport in saturated porous media: Forced-gradient experiment at Borden, Ontario. Water Resour. Res. 33(4), 639-648.

Barb, W.G. and Mikucki, W. 1959. On the coagulation of polymer latices by freezing and thawing. J. Polym. Sci. 37(132), 499-514.

Bense, V. and Kooi, H. 2004. Temporal and spatial variations of shallow subsurface temperature as a record of lateral variations in groundwater flow. J. Geophys. Res. Solid Earth 109(B4).

Bhattacharjee, S. 2016. DLS and zeta potential - What they are and what they are not? J. Control Release 235, 337-351.

Bradford, S.A. and Bettahar, M. 2006. Concentration dependent transport of colloids in saturated porous media. J. Contam. Hydrol. 82(1-2), 99-117.

Bradford, S.A., Yates, S.R., Bettahar, M. and Simunek, J. 2002. Physical factors affecting the transport and fate of colloids in saturated porous media. Water Resour. Res. 38(12), 63-61-63-12.

Busenberg, E., Plummer, N., Doughten, M.W., Widman, P.K. and Bartholomay, R.C. 2000 Chemical and isotopic composition and gas concentrations of ground water and surface water from selected sites at and near the Idaho National Engineering and Environmental Laboratory, Idaho, 1994-97.

Castro, F.D. and Tufenkji, N. 2007. Relevance of nontoxigenic strains as surrogates for *Escherichia coli* O157:H7 in groundwater contamination potential: role of temperature and cell acclimation time. Environ. Sci. Technol. 41(12), 4332-4338.

Chou, K.-S., Liu, H.-L., Kao, L.-H., Yang, C.-M. and Huang, S.-H. 2014. A novel granulation technique using a freeze–thaw method. Ceram. Int. 40(6), 8875-8878.

Derjaguin, B. and Landau, L. 1993. Theory of the stability of strongly charged lyophobic sols and of the adhesion of strongly charged particles in solutions of electrolytes. Prog. Surf. Sci. 43(1-4), 30-59.

Deshiikan, S.R., Eschenazi, E. and Papadopoulos, K.D. 1998. Transport of colloids through porous beds in the presence of natural organic matter. Colloids Surf. A. Physicochem Eng. Asp. 145(1), 93-100.

Domingos, R.F., Baalousha, M.A., Ju-Nam, Y., Reid, M.M., Tufenkji, N., Lead, J.R., Leppard, G.G. and Wilkinson, K.J. 2009. Characterizing manufactured nanoparticles in the environment: multimethod determination of particle sizes. Environ. Sci. Technol. 43(19), 7277-7284.

Duis, K. and Coors, A. 2016. Microplastics in the aquatic and terrestrial environment: sources (with a specific focus on personal care products), fate and effects. Environ. Sci. Eur. 28(1), 2.

Elimelech, M., Gregory, J. and Jia, X. (1995) Particle deposition and aggregation : Measurement, modelling, and simulation, Butterworth-Heinemann, Oxford, England.

Farner, J.M., Cheong, R.S., Mahé, E., Anand, H. and Tufenkji, N. 2019. Comparing TiO2 nanoparticle formulations: stability and photoreactivity are key factors in acute toxicity to Daphnia magna. Environ. Sci. Nano 6(8), 2532-2543.

Farner, J.M., De Tommaso, J., Mantel, H., Cheong, R.S. and Tufenkji, N. 2020. Effect of freeze/thaw on aggregation and transport of nano-TiO2 in saturated porous media. Environ. Sci. Nano.

Franchi, A. and O'Melia, C.R. 2003. Effects of natural organic matter and solution chemistry on the deposition and reentrainment of colloids in porous media. Environ. Sci. Technol. 37(6), 1122-1129.

Hakimzadeh, A., Okshevsky, M., Maisuria, V., Deziel, E. and Tufenkji, N. 2018. Exposure to Freeze-Thaw Conditions Increases Virulence of *Pseudomonas aeruginosa* to *Drosophila melanogaster*. Environ. Sci. Technol. 52(24), 14180-14186.

Halde, R. 1980. Concentration of impurities by progressive freezing. Water Res. 14(6), 575-580.

Hernandez, L.M., Yousefi, N. and Tufenkji, N. 2017. Are there nanoplastics in your personal care products? Environ. Sci. Technol. Lett. 4(7), 280-285.

Hurley, R.R. and Nizzetto, L. 2018. Fate and occurrence of micro(nano)plastics in soils: Knowledge gaps and possible risks. Curr. Opin. in Environ. Sci. Health 1, 6-11.

Johnson, W.P. and Logan, B.E. 1996. Enhanced transport of bacteria in porous media by sediment-phase and aqueous-phase natural organic matter. Water Res. 30(4), 923-931.

Kim, H.N. and Walker, S.L. 2009. *Escherichia coli* transport in porous media: influence of cell strain, solution chemistry, and temperature. Colloids Surf. B. Biointerfaces 71(1), 160-167.

Koelmans, A.A., Mohamed Nor, N.H., Hermsen, E., Kooi, M., Mintenig, S.M. and De France, J. 2019. Microplastics in freshwaters and drinking water: Critical review and assessment of data quality. Water Res. 155, 410-422.

Law, K.L., Moret-Ferguson, S., Maximenko, N.A., Proskurowski, G., Peacock, E.E., Hafner, J. and Reddy, C.M. 2010. Plastic accumulation in the North Atlantic subtropical gyre. Sci 329(5996), 1185-1188.

Liu, D., Johnson, P.R. and Elimelech, M. 1995. Colloid deposition dynamics in flow-through porous media: role of electrolyte concentration. Environ. Sci. Technol. 29(12), 2963-2973.

Lowry, G.V., Hill, R.J., Harper, S., Rawle, A.F., Hendren, C.O., Klaessig, F., Nobbmann, U., Sayre, P. and Rumble, J. 2016. Guidance to improve the scientific value of zeta-potential measurements in nanoEHS. Environmental Science: Nano 3(5), 953-965.

Malvern 2011 Dynamic Light Scattering - Common Terms Defined.

Mattsson, K., Hansson, L.A. and Cedervall, T. 2015. Nano-plastics in the aquatic environment. Environ. Sci. Process Impacts 17(10), 1712-1721.

Mintenig, S.M., Loder, M.G.J., Primpke, S. and Gerdts, G. 2019. Low numbers of microplastics detected in drinking water from ground water sources. Sci. Total Environ. 648, 631-635.

Mitzel, M.R., Sand, S., Whalen, J.K. and Tufenkji, N. 2016. Hydrophobicity of biofilm coatings influences the transport dynamics of polystyrene nanoparticles in biofilm-coated sand. Water Res. 92(7), 113-120.

Nizzetto, L., Futter, M. and Langaas, S. 2016. Are Agricultural Soils Dumps for Microplastics of Urban Origin? Environ. Sci. Technol. 50(20), 10777-10779.

NOAA/NCDC 2000 Engineering Weather Data, Air Force Combat Climatology Center (AFCCC)

Panko, J.M., Chu, J., Kreider, M.L. and Unice, K.M. 2013. Measurement of airborne concentrations of tire and road wear particles in urban and rural areas of France, Japan, and the United States. Atmos. Environ. 72, 192-199.

Panno, S.V., Kelly, W.R., Scott, J., Zheng, W., McNeish, R.E., Holm, N., Hoellein, T.J. and Baranski, E.L. 2019. Microplastic Contamination in Karst Groundwater Systems. Ground Water 57(2), 189-196.

Pelley, A.J. and Tufenkji, N. 2008. Effect of particle size and natural organic matter on the migration of nano- and microscale latex particles in saturated porous media. J. Colloid Interface Sci. 321(1), 74-83.

Petosa, A.R., Jaisi, D.P., Quevedo, I.R., Elimelech, M. and Tufenkji, N. 2010. Aggregation and deposition of engineered nanomaterials in aquatic environments: role of physicochemical interactions. Environ. Sci. Technol. 44(17), 6532-6549.

Petosa, A.R., Öhl, C., Rajput, F. and Tufenkji, N. 2013. Mobility of nanosized cerium dioxide and polymeric capsules in quartz and loamy sands saturated with model and natural groundwaters. Water Res. 47(15), 5889-5900.

Philippe, A. and Schaumann, G.E. 2014. Interactions of Dissolved Organic Matter with Natural and Engineered Inorganic Colloids: A Review. Environ. Sci. Technol. 48(16), 8946-8962.

Pivokonsky, M., Cermakova, L., Novotna, K., Peer, P., Cajthaml, T. and Janda, V. 2018. Occurrence of microplastics in raw and treated drinking water. Sci. Total Environ. 643, 1644-1651.

Probes, M. 2004 Working With FluoSpheres® Fluorescent Microspheres. Technologies, M.P.I.D. (ed).

Quevedo, I.R. and Tufenkji, N. 2012. Mobility of functionalized quantum dots and a model polystyrene nanoparticle in saturated quartz sand and loamy sand. Environ. Sci. Technol. 46(8), 4449-4457.

Rocard, J.M., Asadishad, B., Samonte, P.R.V., Ghoshal, S. and Tufenkji, N. 2018. Natural freeze-thaw cycles may increase the risk associated with *Salmonella* contamination in surface and groundwater environments. Water Res. X 1, 100005.

Saleh, N.B., Pfefferle, L.D. and Elimelech, M. 2010. Influence of biomacromolecules and humic acid on the aggregation kinetics of single-walled carbon nanotubes. Environ. Sci. Technol. 44(7), 2412-2418.

Sasidharan, S., Torkzaban, S., Bradford, S.A., Cook, P.G. and Gupta, V. 2017. Temperature dependency of virus and nanoparticle transport and retention in saturated porous media. J. Contam. Hydrol. 196, 10-20.

Song, Z., Yang, X., Chen, F., Zhao, F., Zhao, Y., Ruan, L., Wang, Y. and Yang, Y. 2019. Fate and transport of nanoplastics in complex natural aquifer media: Effect of particle size and surface functionalization. Sci. Total Environ. 669, 120-128.

Tufenkji, N. and Elimelech, M. 2004. Correlation equation for predicting single-collector efficiency in physicochemical filtration in saturated porous media. Environ. Sci. Technol. 38(2), 529-536.

Tufenkji, N., Miller, G.F., Ryan, J.N., Harvey, R.W. and Elimelech, M. 2004. Transport of Cryptosporidium Oocysts in Porous Media: Role of Straining and Physicochemical Filtration. Environ. Sci. Technol. 38(22), 5932-5938.

Verwey, E.J.W., Overbeek, J.T.G. and Nes, K.v. 1948. Theory of the stability of lyophobic colloids : the interaction of sol particles having an electric double layer.

Wang, M., Gao, B., Tang, D. and Yu, C. 2018. Concurrent aggregation and transport of graphene oxide in saturated porous media: Roles of temperature, cation type, and electrolyte concentration. Environ. Pollut. 235, 350-357.

Wu, J., Jiang, R., Lin, W. and Ouyang, G. 2019. Effect of salinity and humic acid on the aggregation and toxicity of polystyrene nanoplastics with different functional groups and charges. Environ. Pollut. 245, 836-843.

Xiang, H., Chan, D. and Bates, R. 2015. Minimization of Freeze/Thaw-Induced Protein aggregation and optimization of a drug substance formulation matrix. BioPharm. Int. 28(8), 30-37.

Xu, S., Gao, B. and Saiers, J.E. 2006. Straining of colloidal particles in saturated porous media. Water Resources Research 42(12).

Yan, Z., Huang, X. and Yang, C. 2014. Deposition of colloidal particles in a microchannel at elevated temperatures. Microfluid. Nanofluid. 18(3), 403-414.

Yao, K.-M., Habibian, M.T. and O'Melia, C.R. 1971. Water and waste water filtration. Concepts and applications. Environ. Sci. Technol. 5(11), 1105-1112.

Yu, S., Shen, M., Li, S., Fu, Y., Zhang, D., Liu, H. and Liu, J. 2019. Aggregation kinetics of different surface-modified polystyrene nanoparticles in monovalent and divalent electrolytes. Environ. Pollut. 255, 113302.

Zubris, K.A.V. and Richards, B.K. 2005. Synthetic fibers as an indicator of land application of sludge. Environ. Pollut. 138(2), 201-211.

Figure 1

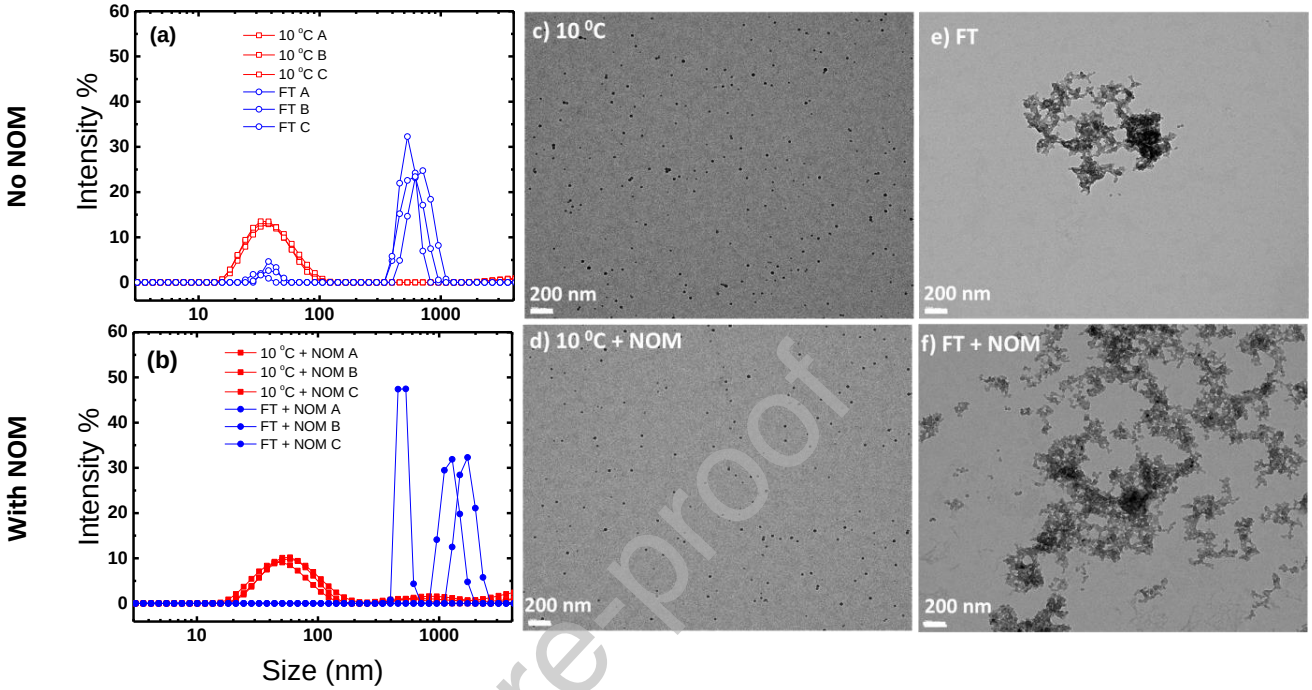

Fig. 1. Representative intensity particle size distribution of nanoplastics in 30 mM NaCl (a) without NOM and (b) in the presence of NOM for three replicate samples (A, B, C). Representative TEM images of nanoplastics kept at 10°C for 240 hours (c and d) and after 10 FT cycles (e and f) all in 30 mM NaCl (a), (c), and (e) are suspensions without NOM. (b), (d), and (f) are suspensions with NOM.

Figure 2

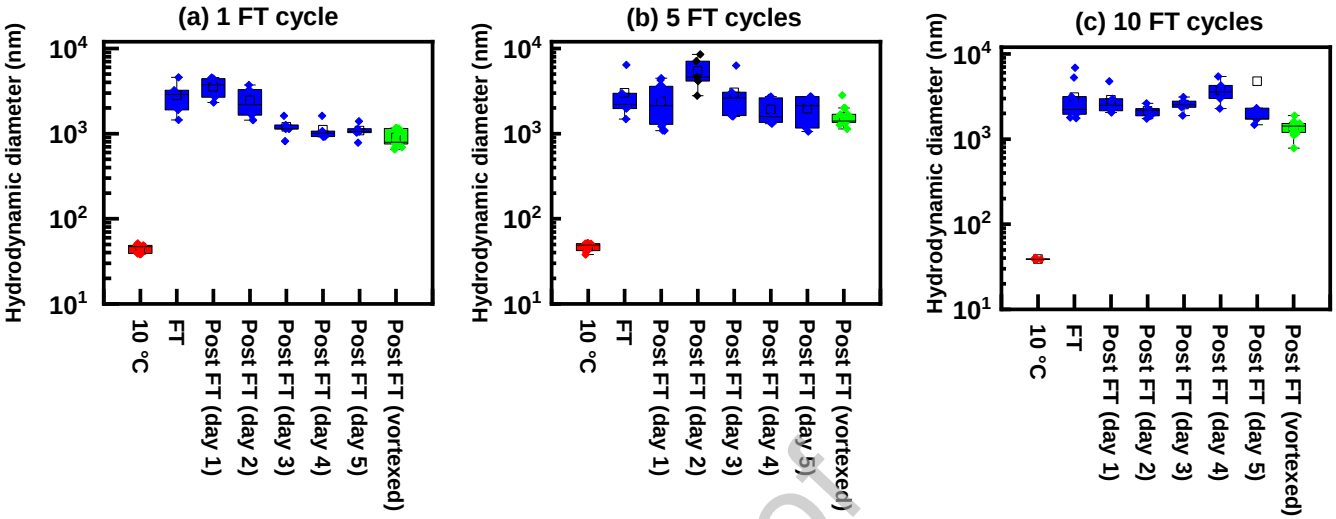

Fig. 2. The stability of the nanoplastic suspension in 10 mM NaCl after exposure to (a) 1 FT cycle (b) 5 FT cycles and (c) 10 FT cycles. Sample stability was measured after FT exposure and named Post FT day 1 – 5. Samples that were vortexed Post FT from day 1 – 5 are collectively plotted as Post FT (vortexed).

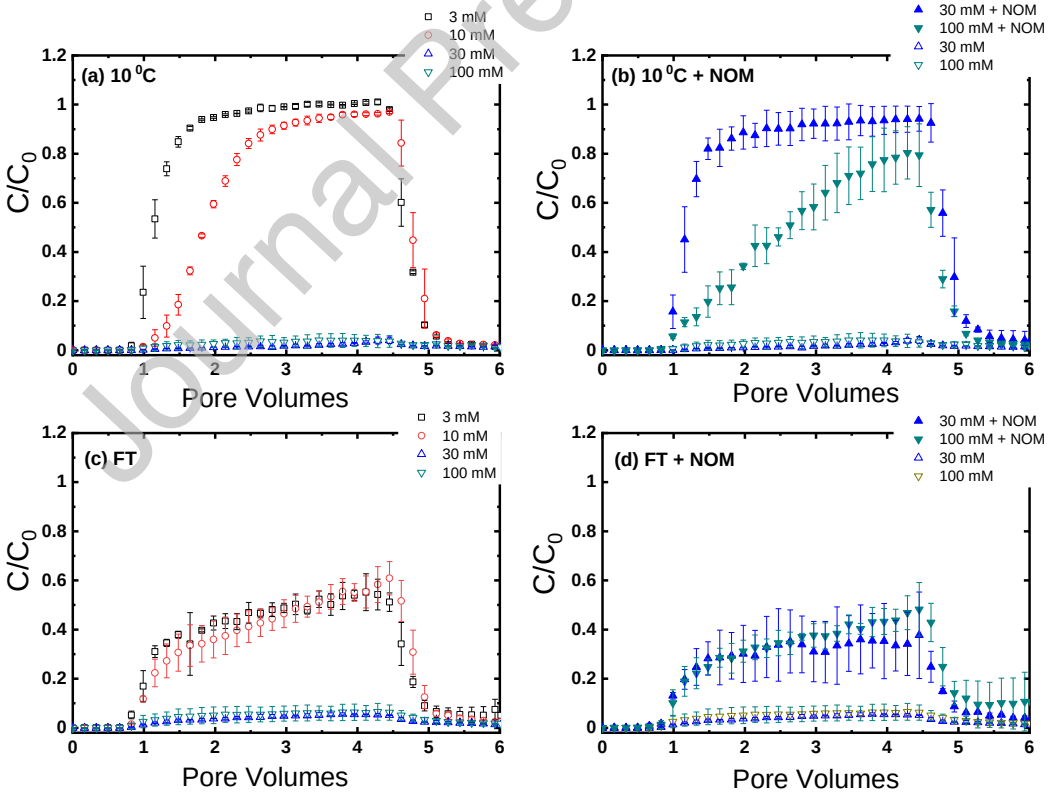

Fig. 3. Breakthrough curves of nanoplastics conducted at (a) 10°C without NOM, (b) 10°C in the presence of NOM, (c) after 10 FT cycles without NOM, (d) after 10 FT cycles in the presence of NOM. Error bars represent standard deviation between duplicate runs.

Figure 4

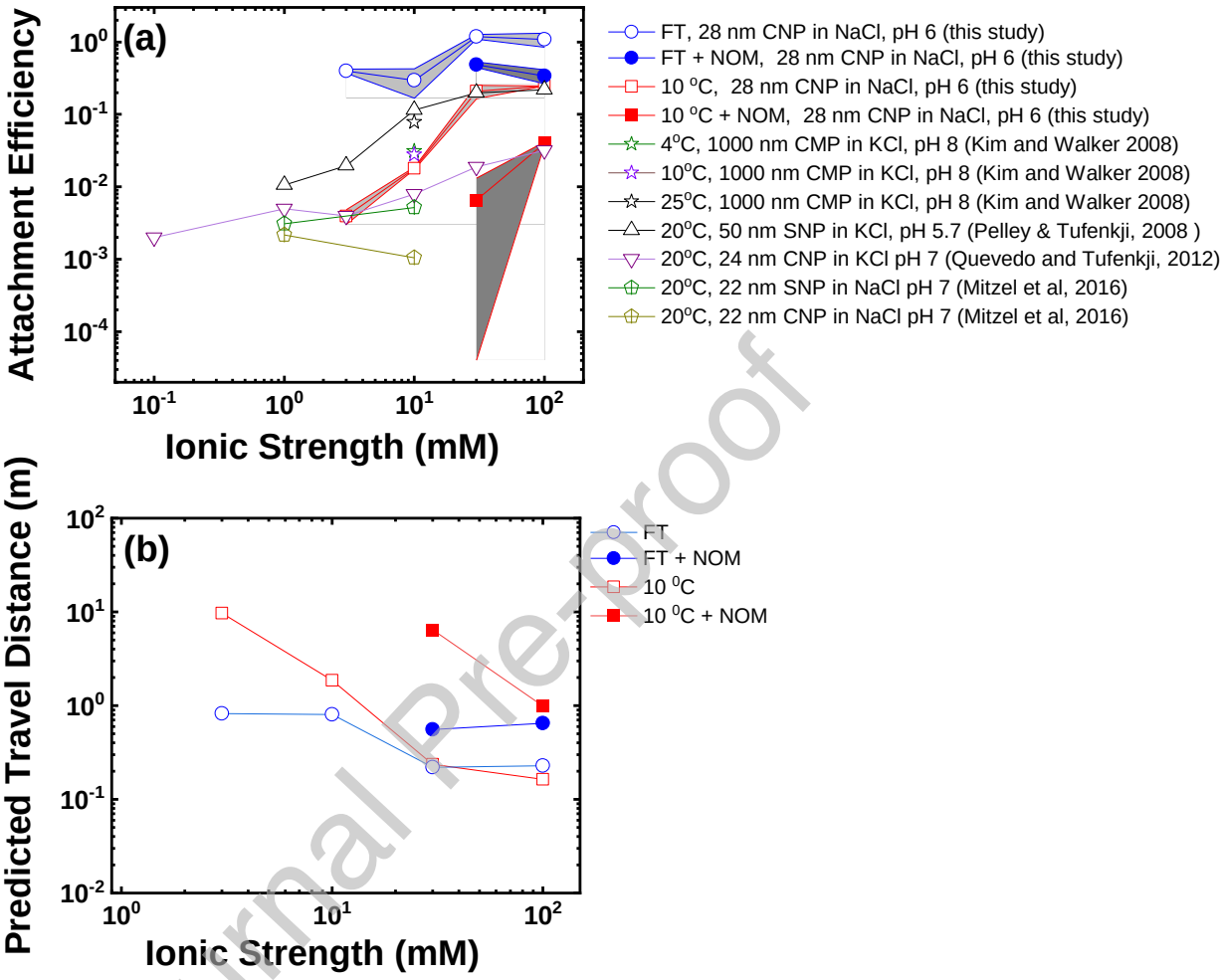

Fig. 4. (a) Attachment efficiency as a function of IS calculated from $d_{h,z\text{-}avg}$ for different nanoplastics and microplastics across different studies. CNP = carboxyl-modified nanoplastic, CMP = carboxyl-modified microplastic, SNP = sulfate-modified nanoplastics. The shaded regions indicate standard deviation (from duplicate measurement) around the mean for this study. Note that values for 4°C and 10°C from Kim and Walker 2008 overlap. (b) Predicted travel distances as a function of ionic strength at both 10°C and FT conditions.

Table 1

Table 1. Measured hydrodynamic diameters, zeta potential (ZP), calculated elution (C/C_0) and attachment efficiencies of the nanoplastics in quartz sand porous media

Particle	Treatment	Ionic strength (mM NaCl)	C/C_0	$d_{h,\ z\text{-}avg}$ (nm)	PDI	$d_{h,\ intensity}$ (nm)	$d_{h,\ volume}$ (nm)	$\alpha_{z\text{-}avg}$	$\alpha_{int\ mean}$	ZP (mV)
Nanoplastics	10°C	3	0.95	55 ± 2	0.29	80 ± 3	50 ± 4	$0.0040 \pm 9.1\times10^{-4}$	$0.0039 \pm 9.0\times10^{-4}$	-22.1 ± 2.5
		10	0.72	46 ± 4	0.27	55 ± 4	43 ± 2	$0.018 \pm 6.4\times10^{-4}$	$0.021 \pm 5.7\times10^{-4}$	-25.5 ± 5.4
		30	0.024	46 ± 10	0.24	55 ± 16	43 ± 9	$0.21 \pm 4.4\times10^{-2}$	$0.24 \pm 6.4\times10^{-2}$	-22.5 ± 5.9
		100	0.026	58 ± 4	0.30	61 ± 8	66 ± 2	$0.25 \pm 0.0\times10^{0}$	$0.27 \pm 3.0\times10^{-2}$	-15.2 ± 1.1
	FT	3	0.49	1044 ± 156	0.81	462 ± 163	486 ± 94	$0.40 \pm 2.5\times10^{-2}$	$0.24 \pm 3.3\times10^{-2}$	-27.9 ± 7.0
		10	0.47	582 ± 331	0.73	407 ± 136	402 ± 221	$0.30 \pm 1.3\times10^{-1}$	$0.24 \pm 3.1\times10^{-2}$	-35.6 ± 6.5
		30	0.070	668 ± 85	0.76	687 ± 124	281 ± 28	$1.1 \pm 9.3\times10^{-2}$	$1.2 \pm 5.6\times10^{-2}$	-23.4 ± 1.5
		100	0.063	612 ± 353	0.78	484 ± 118	194 ± 15	$1.1 \pm 2.4\times10^{-1}$	$1.0 \pm 3.6\times10^{-1}$	-20.2 ± 1.8
Nanoplastics + NOM	10°C	30	0.92	65 ± 10	0.36	66 ± 17	71 ± 20	$0.0066 \pm 6.9\times10^{-3}$	$0.0070 \pm 7.6\times10^{-3}$	-55.5 ± 7.2
		100	0.54	57 ± 13	0.33	70 ± 28	72 ± 27	$0.040 \pm 1.8\times10^{-3}$	$0.047 \pm 4.8\times10^{-3}$	-15.0 ± 4.1
	FT	30	0.47	2834 ± 1585	0.82	483 ± 121	475 ± 139	$0.49 \pm 4.2\times10^{-2}$	$0.41 \pm 2.0\times10^{-1}$	-34.9 ± 9.3
		100	0.38	519 ± 134	0.60	384 ± 32	405 ± 9	$0.34 \pm 7.5\times10^{-2}$	$0.29 \pm 2.8\times10^{-2}$	-20.4 ± 2.7

GRAPHICAL ABSTRACT